The increased interface charge transfer in dye-sensitized solar cells based on well-ordered TiO_2 nanotube arrays with different lengths

Lihong Qi,[a] Zhuoxun Yin, Shen Zhang, Qiuyun Ouyang, Chunyan Li, and Yujin Chen
College of Science, Harbin Engineering University, Harbin 150001, People's Republic of China

(Received 16 January 2014; accepted 10 February 2014)

The well-ordered TiO_2 nanotube arrays with controlled aspect ratio are fabricated via potentiostatic anodization. The aspect ratio of TiO_2 nanotube array can be tuned conveniently by changing the water content in electrolyte and anodization time. The formation of well-ordered TiO_2 nanotube array is good for the photogenerated electron transfer. So, the well-ordered TiO_2 nanotube array photoelectrodes have been used to fabricate dye-sensitized solar cells (DSSCs). It is found that, with the optimum nanotube length and aspect ratio, DSSCs with TiO_2 nanotube array photoelectrodes show better photoelectric conversion efficiency (2.60%) than that with TiO_2 nanoparticles on Ti foil photoelectrode. It is elucidated by the interfacial electron transport of DSSCs, which are characterized quantitatively, using the electrochemical impedance spectra. The DSSC with optimal nanotube length and aspect ratio displays the fastest interfacial electron transfer and longer electron lifetime.

I. INTRODUCTION

Since the pioneering work of M. Grätzel in 1991, the dye-sensitized solar cells (DSSCs) have attracted more attention due to their intrinsic advantages of low cost, non-pollution, easy production, and relatively high power conversion efficiency (η).[1–4] Generally, DSSCs consist of nanocrystalline semiconductor oxide photoelectrode, dye sensitizer, redox shuttle electrolyte, and counter electrode. Under illumination, electron is injected into the conduction band of the semiconductor photoelectrode from the excited state of the sensitizer. A suitable redox shuttle electrolyte can recover the oxidized dye. The diffusion of the oxidized shuttle electrolyte to the counter electrode completes the circuit.[5–7] In principle, fast photoelectron transfer and slow recombination will bring about a high η. It has been established that the structural and physical properties of the nanocrystalline semiconductor oxide are predominant factors.[8]

An anatase TiO_2 nanoparticle (NP) film is a commonly used photoelectrode for DSSCs due to its facile fabrication and low cost.[9–11] However, its small electron diffusion coefficient limits the random walk of electrons through the NP film.[12] Some strategies have been tried to optimize the structure of the photoelectrodes to increase the photoelectron transfer and reduce the charge recombination. One strategy is to apply one-dimensional (1D) nanomaterials including nanowires, nanotubes, nanorods, and nanofibers because these materials can accelerate electron transport and increase light scattering.[13–15] Unfortunately, these 1D nanomaterials commonly suffer from random array patterns, which cannot reduce the recombination significantly and thus result in a lower η.[16] Highly ordered TiO_2 nanotubes may provide an alternative electron transport material that reduces charge recombination and increases electron collection relative to conventional disordered NP or random 1D nanomaterial channels.[17–20] However, the η of DSSCs based on TiO_2 nanotubes remained relatively low as a result of incomplete coverage of dye molecules on the TiO_2 nanotube surface and insufficient infiltration of electrolyte into TiO_2 nanotubes.[21–24] So, fabrication of well-ordered semiconductor oxide array photoelectrodes with optimized structural parameters and surface properties is a better method to increase the photoelectron transfer and reduce the recombination of DSSCs.

Herein, the highly ordered TiO_2 nanotube arrays with controlled aspect ratio were prepared via potentiostatic anodization. And the controllable aspect ratio of TiO_2 nanotube arrays can be achieved by only changing the water content and anodization time. Then, the DSSCs based on the highly ordered TiO_2 nanotube array photoelectrodes were fabricated. The DSSCs based with optimal aspect ratio possessed the highest η of 2.60% under backside illumination. This is because the optimal aspect ratio of TiO_2 nanotube arrays could result in a better separation of photogenerated charges. Meanwhile, the influence of different aspect ratios on the η has been systematically investigated by the electrochemical impedance spectra (EIS).

II. EXPERIMENTAL DETAILS

A 0.25-mm-thick titanium foil (99.7%, Aldrich), HF (40%), ammonium fluoride (97.0%), formamide (98.5%),

[a]Address all correspondence to this author.
e-mail: lihongqi@hrbeu.edu.cn
DOI: 10.1557/jmr.2014.50

 © Materials Research Society 2014

https://doi.org/10.1557/jmr.2014.50 Published online by Cambridge University Press

and commercial TiO_2 powder (P25, Degussa, Germany) were purchased from standard sources and used as received. The transparent conducting glass (TCO, 20 Ω/square, Nippon sheet glass, Japan) was used as received for electrode substrate. The used Ru complex dye was cis-bis (isothiocyanato) bis(2,2′-bipyridyl-4,4′-dicarboxylato) ruthenium(II)bistetrabutyl-ammonium (N719, Solaronix SA, Switzerland). The redox shuttle electrolyte was composed of 0.1 M LiI (anhydrous, 99%, Acros), 0.05 M I_2 (≥99.8%), 0.5 M tert-butylpyridine (99%, Aldrich), and 0.6 M 1-propyl-2,3-dimethylimidazolium iodide (99%) in acetonitrile (99%, Fluka). All the other solvents and chemicals used in the experiments are at least reagent grade and used as received. Milli-Q water with a resistivity of 18 MΩ cm was used in all the experiments.

Highly ordered TiO_2 nanotube arrays were prepared by a potentiostatic anodization with a two-electrode electrochemical cell. The titanium foil was used as a working electrode, and a platinum foil served as a counter electrode. The interval between the working electrode and counter electrode was approximately 2.5 cm. The voltage was applied by a DC power supply (model DYY-6C, Beijing 61 Technology, P.R. China). A short TiO_2 nanotube array was formed by anodizing the Ti foil in 40 mL of 0.5 wt% HF solution at 20 V for 20 min, which is the same as the reported method.[25,26] Other TiO_2 nanotube arrays were prepared at the same applied voltage (20 V) by using 40 mL of organic electrolyte. The present organic electrolyte was 0.27 M ammonium fluoride (97.0%, Wako Chemicals) in formamide (98.5%, Wako Chemicals) containing different water content (3% and 4%) respectively. The aspect ratio of the nanotube array could be controlled using different water content and anodization time (1 h or 6 h). This is similar to the report of Grimes et al. and Liu et al., with only a slight change of water content.[25,26] Broken nanotubes and fragments were formed generally on the surface of the nanotube array and could be removed by washing in isopropyl alcohol ultrasonically. The TiO_2 NPs (P25) with the thickness of 10 μm were also coated on Ti foil via doctor blade method for comparison. The crystallization of TiO_2 nanotube array and TiO_2 NP photoelectrodes were realized by annealing the as-prepared film at 500 °C under ambient air for 3 h.

The sensitization of the prepared TiO_2 nanotube array and TiO_2 NP photoelectrodes was achieved by immersing them into 0.5 mM N719 dye solution for 24 h. The counter electrode was prepared according to the previous work.[27] The dye-sensitized TiO_2 nanotube array and TiO_2 NP photoelectrodes with Pt counter electrodes were adhered together with epoxy resin, respectively. The space between the electrodes was filled with the electrolyte by capillary action.

X-ray powder diffraction (XRD) patterns were obtained by a Rigaku D/max-IIIB diffractometer using Cu K_α radiation ($\lambda = 0.15406$ nm). Scanning electron microscopy (SEM) images were recorded using a Hitachi S-4800 instrument operating at 15 kV. The amount of adsorbed dye was measured by immersing dye-sensitized photoelectrodes in a 0.02 M NaOH solution in alcohol and water (volume ratio 1:1) for 6 h. Then the resulting solution was quantified with the UV-vis spectrophotometer (Shimadzu UV-2550, Kyoto, Japan).

Photocurrent–photovoltage curves (J–V) were recorded by a BAS100B electrochemical analyzer (Bioanalytical Systems Inc., West Lafayette, Indiana). A 400 W xenon lamp with a UV filter was used as the light source. Its illumination intensity was about 40 mW cm^{-2}. The irradiation area of DSSCs was about 0.12 cm^2. The EIS were performed with a computer-controlled IM6e impedance measurement unit (Zahner Elektrik, Kronach, Germany). EIS were obtained by applying sinusoidal perturbations of 10 mV over the V_{oc} at the frequency range from 0.05 to 100 kHz. All EIS measurements were carried out under illumination of 10 mW cm^{-2}. The obtained spectra were fitted with ZsimpWin software in terms of appropriate equivalent circuits.

III. RESULTS AND DISCUSSION

The formation of TiO_2 nanotube arrays in the electrolyte containing fluoride ion is a result of the interactions between three simultaneously occurring processes, namely the electrical field assisted oxidation of Ti metal to form TiO_2, the field assisted dissolution of Ti metal ions into the electrolyte, and the chemical dissolution of Ti and TiO_2 due to fluoride ion etching, which is substantially enhanced by the presence of H^+ ion. So, the concentrations of H^+ and F^- ions are the important parameters for obtaining well-ordered TiO_2 nanotube arrays.[28]

The current voltage behavior of HF solutions and electrolyte containing fluoride ion with different water content was probed at 22 °C under DC conditions using planar platinum electrodes with a measured cell constant of 2.5 (ratio of the distance between the two electrodes divided by their area) and readings were recorded; these data are shown in Fig. 1. It can be clearly seen that the current density of electrolyte containing fluoride ion increased with the increase of water content in it. And the current density of HF solution is similar to that of electrolyte containing fluoride ion with 40% water content when the applied bias is lower than 20 V. More water content in the electrolyte results in faster dissolution of Ti metal ions. This means that water content in the electrolyte has an important impact on the field-assisted dissolution of Ti metal ions. So, the HF solution and electrolyte containing fluoride ion with water content of 3% and 4% have been selected for preparation of TiO_2 nanotube arrays with controlled aspect ratio in the potentiostatic anodization process. The growth of TiO_2 nanotube arrays was studied in fluoride-bearing electrolytes containing different water

https://doi.org/10.1557/jmr.2014.50 Published online by Cambridge University Press

content while maintaining similar molar concentrations of the chemical species. This ensured that each electrolyte had the same concentration of fluoride ions, thus allowing us to observe the effect of the water content on nanotube growth. Meanwhile, the effect of different anodization time on the growth of TiO_2 nanotubes was also studied. Figure 2 shows the real-time potentiostatic anodization behavior of Ti anodized at 20 V in formamide solutions containing 0.27 M of NH_4F with different water content and different anodization time, respectively. In the HF solution, the anodization current drops sharply from a high value into a low value during the first 5 s of anodization time. Then, the anodization current increases to reach a stable value after approximately 500 s (Fig. S1). In the first anodization stage, the formation of insulation TiO_2 oxide layer results in decrease of current. Then, pitting the oxide layer by fluoride ions occurs, which makes the current increase to a stable value. On the other hand, the anodization current in the electrolytes containing formamide remains relatively constant during the first 20–30 s of anodization. The region of stable current extends for a longer period of time in electrolytes containing a smaller concentration of water. Then the current decreases monotonically to reach a stable value. During the initial anodization period, the current is bigger and the escape of gas from the anode can be seen. Because the gas formation is an electronic charge transfer process, electronic conduction possibly dominates in the early anodization stage. The donation of oxygen is more difficult compared to water in organic electrolytes and this is not favorable to form TiO_2 barrier layer. The reduction in water content results in thinner barrier layers, which maybe enhances the ionic transfer through them (Fig. 2). The faster ionic transfer rate is advantageous to faster movement of the Ti/TiO_2 interface into the Ti substrate for the formation of a longer nanotube array. Longer anodization time also provides a greater driving force for both electronic and ionic conduction for longer nanotube length.

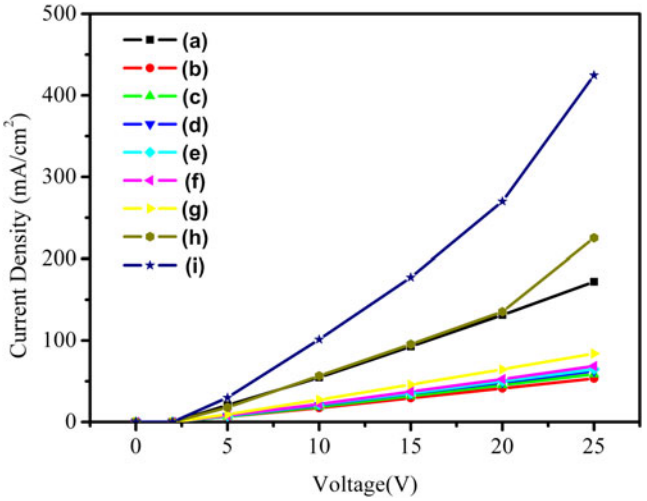


FIG. 1. Current voltage behavior of HF solution (a) and electrolytes containing fluoride ion with different water content of 1% (b), 2% (c), 3% (d), 4% (e), 5% (f), 10% (g), 40% (h), 100% (i) probed by using planar platinum electrodes with a cell constant of 2.5 (ratio of the distance between the two electrodes divided by their area).

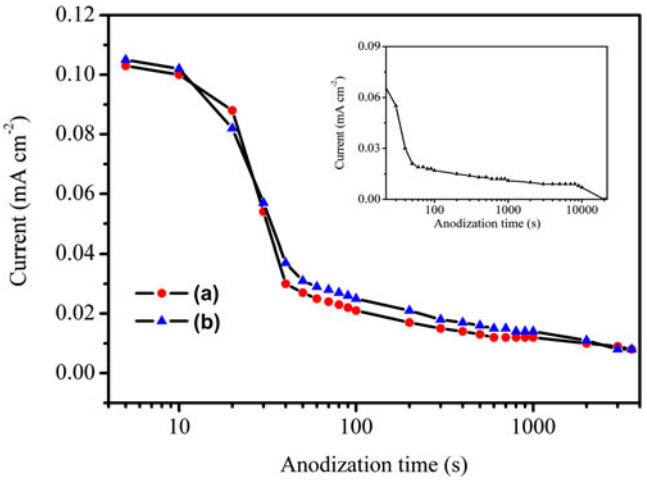


FIG. 2. Current-time behavior during 20 V potentiostatic anodization of a Ti foil in a formamide solution containing identical molar concentrations (0.27 M) of fluoride ion with controllable H_2O content of 3% (a), 4% (b) for 1 h. Inset: Current-time behavior during 20 V potentiostatic anodization of a Ti foil in a formamide solution containing identical molar concentrations (0.27 M) of fluoride ion with controllable H_2O content of 3% for 6 h.

The surface morphology is a function of anodization time in electrolytes containing different water content. SEM images of the anodic TiO_2 films formed in the 0.27 M ammonium fluoride in formamide solution containing different water content (3% and 4%) for different anodization time are shown in Fig. 3. It can be seen that the TiO_2 nanotube arrays with the pore diameter remaining roughly constant (approximately 100 nm) have been obtained [Figs. 3(a), 3(c), and 3(e)]. Anodization in HF solution can only obtain similar nanotube array with similar pore diameter (Fig. S2). By controlling the water content (3% and 4%) in the electrolyte, the nanotube array with a length of 4 μm and 3.5 μm (aspect ratio of 40 and 35) can be obtained, respectively [Figs. 3(b) and 3(d)]. As the water content increases in organic electrolyte, the length of TiO_2 nanotube arrays decreased. Meanwhile, by changing the anodization time to 6 h in formamide solution with water content of 3%, the nanotube array with a length of 10 μm (aspect ratio of 100) can also be fabricated [Fig. 3(f)]. But in HF solution, short TiO_2 nanotube array with approximately 0.2 μm length could be obtained according to the report of Ref. 26 , As the H^+ concentration is different due to different water content in the formamide-based electrolyte, the chemical dissolution rate of TiO_2 is different, and thus a long nanotube structure with different lengths can form. However, in the HF electrolyte solution, the high H^+ concentration will make the chemical dissolution of TiO_2

https://doi.org/10.1557/jmr.2014.50 Published online by Cambridge University Press

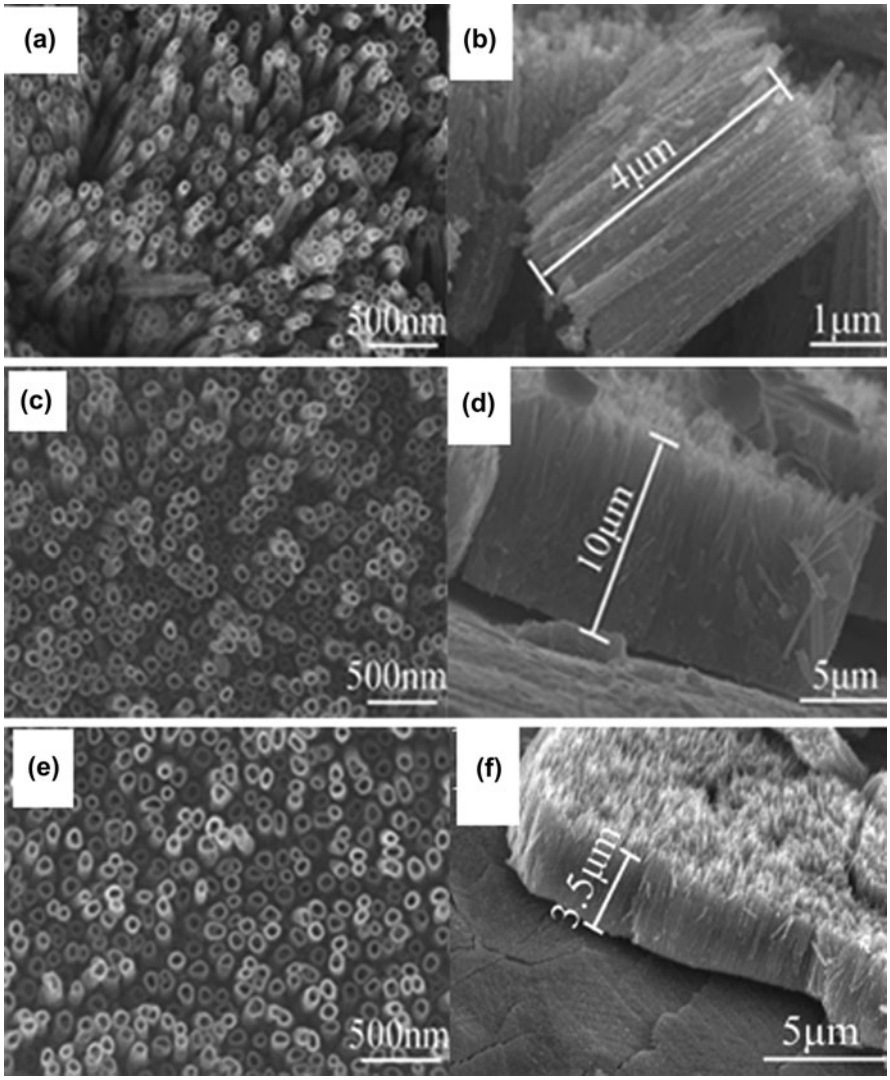


FIG. 3. Top view and cross-sectional images of TiO_2 nanotubes arrays prepared by anodizing Ti foil at 20 V in formamide-based electrolyte with water content 3 wt% for 1 h (a, b), 3 wt% for 6 h (c, d) and formamide-based electrolyte with water content of 4 wt% for 1 h (e, f).

by fluoride ions very quick, resulting in a short nanotube. Anyway, by controlling the water content and anodization time, the TiO_2 nanotube arrays with different lengths and aspect ratios (40, 35, and 100) have been obtained.

Figure 4 shows the typical XRD patterns of as-prepared TiO_2 nanotube array samples with different lengths, respectively. After being annealed at 500 °C under ambient air for 3 h, the anatase TiO_2 pattern is formed, whose diffraction peaks at 25.5°, 37.3°, 38.1°, and 48.2° of 2θ correspond to (101), (103), (004), and (200) plane of anatase TiO_2 (JCPDS, No. 21-1272). All the obtained TiO_2 nanotube arrays show high crystalline degree after annealed.

The current density–voltage (J–V) characteristics for the masked DSSCs with different lengths TiO_2 nanotube array photoelectrodes are presented in Fig. 5. The values of open circuit voltage (V_{oc}), short-circuit current (J_{sc}), fill factor (FF), and overall conversion efficiency (η), obtained from the curves of solar cells, are shown in Table I. Each value for cell performance is determined as an average of at least three samples. The DSSCs based on TiO_2 nanotube array photoelectrodes with lengths of 3.5 μm, 4 μm, and 10 μm have η of 1.42%, 1.59%, and 2.60%, respectively. It can be clearly seen that the η increases with increasing nanotube length. Compared with η of the DSSCs based on the TiO_2 NP photoelectrode on Ti foil (1.77%), the DSSCs based on TiO_2 nanotube array photoelectrodes with length of 10 μm have higher η. This is due to the well-ordered nanotube array structure, which can accelerate the photogenerated electron transfer into the out circuit. However, because of the illumination at the backside, the η of these devices is relatively lower compared with the illumination at the front side. The Pt-coated counter electrodes partially reflect light,

https://doi.org/10.1557/jmr.2014.50 Published online by Cambridge University Press

and the redox shuttle electrolyte absorbs photons in the near-UV region, which decreased light harvesting.

It is believed that the photoelectrochemical properties of DSSCs are correlated with the dye adsorption amount and interface charge transfer rate.[29] More dye adsorption amount and faster interfacial charge transfer will result in higher η. The dye loading/unloading measurement is carried out to determine the dye adsorption amount. According to Lambert–Beer's law, the molar concentration of dye unloading from TiO_2 nanotube arrays with lengths of 3.5 μm, 4 μm, 10 μm and NP photoelectrode on Ti foil is 1.9, 1.9, 2.3, and 2.6 × 10^{-8} mol cm^{-2}, respectively (Fig. 6). Although the TiO_2 nanotube arrays have lower dye adsorption amount than TiO_2 NP photoelectrode, DSSC based on TiO_2 nanotube arrays with the length of 10 μm has better η than DSSC based on NP photoelectrodes. Therefore, we do not think the improved η results from the amount of adsorbed dye molecules. This demonstrates that the length and aspect ratio of TiO_2 nanotube arrays play a significant role in determining the η of DSSCs. The choice of TiO_2 nanotube array structures with a proper length and aspect ratio can effectively improve the performance of DSSCs. In the following, we used EIS to investigate the interfacial charge transport rate in TiO_2 nanotube array structures.

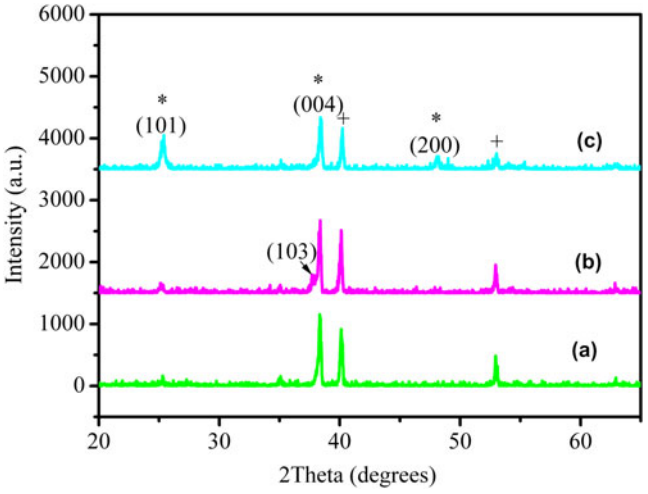


FIG. 4. X-ray diffraction patterns of TiO_2 nanotube arrays with tube lengths of 4 μm (a), 3.5 μm (b), and 10 μm (c) (*: anatase phase diffraction patterns; +: Ti foil diffraction patterns).

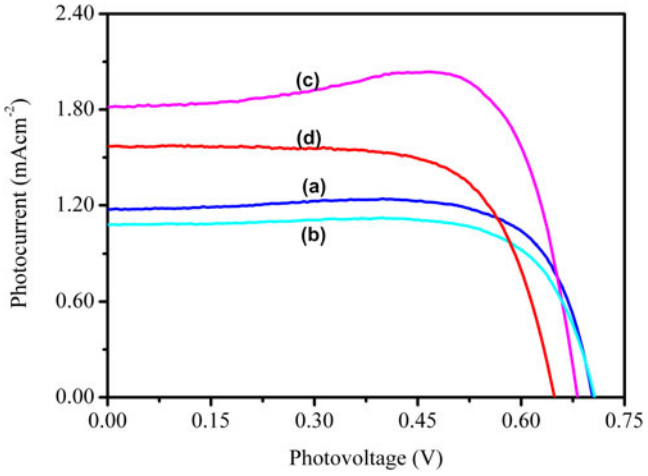


FIG. 5. *J–V* curves of DSSCs based on the ordered TiO_2 nanotube array photoelectrodes with tube lengths of 4 μm (a), 3.5 μm (b), 10 μm (c) and photoelectrode with TiO_2 NPs coated on Ti foil (d).

TABLE I. Solar cell parameters of DSSCs based on TiO_2 nanotube array photoelectrodes and coated-on Ti foil TiO_2 nanoparticle photoelectrode.

DSSCs	V_{oc} (V)	J_{sc} (mA cm^2)	FF	η (%)
DSSCs with 4 μm nanotube	0.704	1.174	0.77	1.59
DSSCs with 3.5 μm nanotube	0.706	1.078	0.75	1.42
DSSCs with 10 μm nanotube	0.682	1.817	0.84	2.60
DSSCs with 10 μm TiO_2 nanoparticles	0.648	1.572	0.69	1.77

EIS is one of the powerful tools to investigate internal resistances of DSSCs that reflect the charge transfer process. DSSC is a complex system composed of several interfaces. A high electron accumulation must have occurred under illumination. Electron transport and recombination in photoelectrode, charge transfer process at Pt counter electrode, and the diffusion constant of I_3^- can all be studied by EIS.[30] Usually, the impedance at low frequency (0.05–1 Hz) corresponds to the Nernst diffusion of I_3^-/I^- within the electrolyte. The impedance at high frequency (1–100 kHz) in the impedance spectra corresponds to the capacitance and charge-transfer resistance at the Pt | I_3^-/I^- electrolyte interface. The medium-frequency response at 1–1 kHz is associated with the

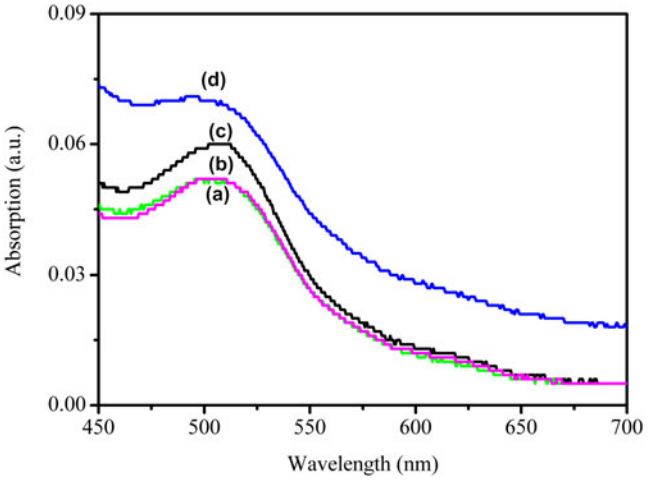


FIG. 6. Optical absorbance of solutions containing dyes detached from the well-ordered TiO_2 nanotube arrays with tube lengths of 4 μm (a), 3.5 μm (b), 10 μm (c), and photoelectrode with TiO_2 NPs coated on Ti foil (d), respectively.

https://doi.org/10.1557/jmr.2014.50 Published online by Cambridge University Press

photoelectrode-dye | I_3^-/I^- electrolyte interface, where an accumulation of photoelectrons is expected. Figure 7 shows the Nyquist diagrams of the impedance spectra of DSSCs based on TiO_2 nanotube arrays with lengths of 3.5 μm, 4.0 μm, 10 μm and TiO_2 NPs on Ti foil under illumination of 10 mW cm^{-2}.

In general, the Nyquist diagram obtained under light intensity of 100 mW cm^{-2} exhibits three semicircles, which corresponds to three frequency ranges. However, in this experiment, only the semicircles at middle and high frequencies are observed, associated with the dye-sensitized photoelectrode | I_3^-/I^- electrolyte interface and the Pt | I_3^-/I^- electrolyte interface resistance, respectively. The semicircle at low frequency region merges with the semicircle at the middle frequency region due to weak light intensity.[29]

The equivalent model fitting the impedance spectra of DSSCs based on TiO_2 nanotube arrays with lengths of 3.5 μm, 4.0 μm, 10 μm and TiO_2 NPs on Ti foil is shown in Fig. 8. The symbols of R and C represent a resistance and a capacitance, respectively. R_1 is a series resistance standing for the transport resistance between the Ti foil and TCO electrode. If the thickness of the TiO_2 nanotube arrays is L, the R_{ct} ($=r_{ct}/L$) represents the charge transfer resistance between photoelectrode and I_3^-/I^- in electrolyte. C_1 ($=c_1L$) is the chemical capacitance of the TiO_2 nanotube array photoelectrode that accounts for the change of electron density as a function of the Fermi level. Z_{Dif} represents the Warburg impedance relative to the Nernst diffusion of I_3^- in electrolyte, where the impedance of the finite-length Warburg diffusion can be expressed by

$$Z_{Dif} = R_{Dif}\left\{\left[\tanh\left(jw\tau\right)^{1/2}\right]\Big/\left(jw\tau\right)^{1/2}\right\}$$

where $R_{Dif} = B/Y_{O1}$, $\tau = B^2$, B is the parameter. R_2 and C_2 are the charge-transfer resistance and double-layer capacitance at the counter electrode, respectively.

The EIS data are obtained by fitting the impedance spectra of DSSCs based on TiO_2 nanotube arrays with lengths of 3.5 μm, 4.0 μm, 10 μm and TiO_2 NPs on Ti foil. R_{ct} represents interfacial resistance of the dye-sensitized photoelectrode | I_3^-/I^- electrolyte interface. Less interface resistance will result in faster interfacial electron transfer, which favors the higher η. Among them, the DSSCs based on 10 μm TiO_2 nanotube arrays display the fastest electron transfer rate (52 Ω), and thus the highest η. When the well-ordered TiO_2 nanotube arrays are used as photoelectrodes, and the photoelectrons tend to undertake a convenient transfer path. That is, electrons transfer through the TiO_2 nanotube array into the external circuit, which would reduce the probability that the photoelectrons are trapped by the NP boundary. So the R_{ct} decreases. But, when the TiO_2 NPs on Ti foil are used as photoelectrode, more particle boundaries are formed. More particle boundaries would result in the photoelectrons trap during the transport, so the R_{ct} increases (272 Ω). These results are also supported by their corresponding Bode diagrams (Fig. 9). The position of the characteristic frequency peak is shifted to a lower frequency (from 0.48 to 0.12 Hz). Any shift of the peak from high frequency to low frequency reveals a more rapid electron transport process due to longer electron lifetime (τ), because the value (f_{mid}) of the middle frequency is related to the inverse of τ as follows: $\tau = 1/(2\pi f_{mid})$. For the DSSCs based on the TiO_2 nanotube array with length of 10 μm, longer electron lifetime (1.28 s) is obtained compared with 0.42 s for the DSSCs based on the TiO_2 NPs on Ti foil, 0.38 s for the DSSCs based on 4 μm nanotube array and 0.33 s for the DSSCs based on 3.5 μm nanotube array. Therefore, the Nyquist and Bode diagrams show that increasing nanotube array length could greatly improve the electrochemical activity due to the prolonged τ. In other words, the

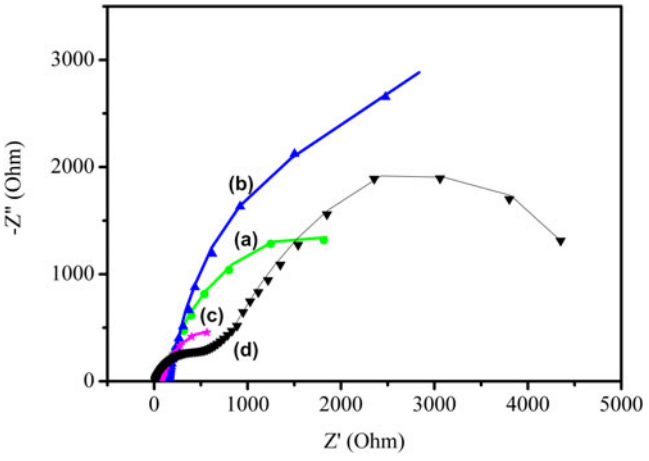


FIG. 7. Nyquist diagrams of the impedance spectra of DSSCs based on TiO_2 nanotube array photoelectrode with lengths of 4 μm (a), 3.5 μm (b), 10 μm (c) and DSSC based on photoelectrode with TiO_2 NP coated on Ti foil (d).

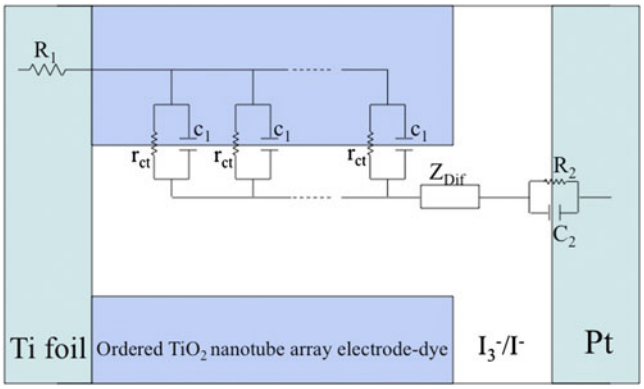


FIG. 8. The equivalent model used to represent interfaces in DSSCs composed of Ti foil | ordered TiO_2 nanotube array photoelectrode-dye | I_3^-/I^- || Pt | TCO.

https://doi.org/10.1557/jmr.2014.50 Published online by Cambridge University Press

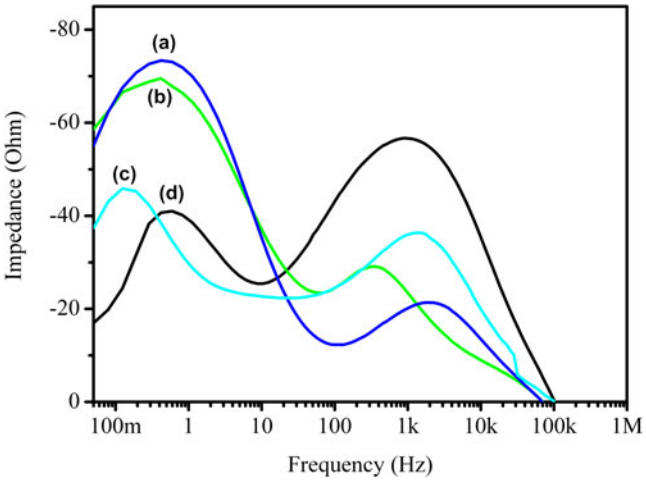


FIG. 9. Bode diagrams of the impedance spectra of DSSCs based on TiO_2 nanotube array photoelectrode with length of 4 μm (a), 3.4 μm (b), 10 μm (c) and photoelectrode with TiO_2 NP coated on Ti foil (d).

electrons with longer τ can obtain longer effective diffusion length and more easily escape the electron recombination. These results are in accordance with photoelectrical conversion efficiency data discussed above.

IV. CONCLUSIONS

In this present work, the conversion efficiency of DSSCs was improved by using well-ordered TiO_2 nanotube array photoelectrode with long nanotube length, which can effectively increase the photoelectron transfer and reduce the recombination of DSSCs. The nanotube length of TiO_2 nanotube array photoelectrode is demonstrated to have a significant influence on the η of DSSCs. The cell based on the TiO_2 nanotube array photoelectrode with nanotube length of 10 μm achieves the highest η of 2.60%, superior to 1.77% of the TiO_2 NPs on Ti foil cells. Such an improved η of the TiO_2 nanotube array cells with nanotube length of 10 μm is ascribed to the fastest interfacial electron transfer and longer electron lifetime, as evidenced by the measurement of the EIS.

ACKNOWLEDGMENTS

This work was supported by the National Natural Science Fund of China (Grant Nos. 51302047, 51072038, 51272050, and 61205113), the Program for New Century Excellent Talents in University (NECT-10-0049), the Outstanding Youth Fund of Heilongjiang Province (Grant No. JC201008), the 111 project (B13015) of Ministry Education of China to the Harbin Engineering University, and also the Fundamental Research Funds for the Central Universities of China for the financial support of this research.

REFERENCES

1. B. O'Regan and M. Grätzel: A low-cost, high-efficiency solar cell based on dye-sensitized colloidal TiO_2 films. *Nature* **353**, 737 (1991).
2. U. Bach, D. Lupo, P. Comte, J-E. Moser, F. Weissortel, J. Salbeck, H. Spreitzer, and M. Grätzel: Solid-state dye-sensitized mesoporous TiO_2 solar cells with high photon-to-electron conversion efficiencies. *Nature* **395**, 583 (1998).
3. M. Grätzel: Recent advances in sensitized mesoscopic solar cells. *Acc. Chem. Res.* **42**, 1788 (2009).
4. A. Yella, H-W. Lee, H-N. Tsao, C. Yi, A-K. Chandiran, M-K. Nazeeruddin, E-W. Diau, C-Y. Yeh, S-M. Zakeeruddin, and M. Grätzel: Porphyrin-sensitized solar cells with cobalt (II/III)–based redox electrolyte exceed 12 percent efficiency. *Science* **334**, 629 (2011).
5. Y-J. Kim, M-H. Lee, H-J. Kim, G. Lim, Y-S. Choi, N. Park, K. Kim, and W-I. Lee: Formation of highly efficient dye-sensitized solar cells by hierarchical pore generation with nanoporous TiO_2 spheres. *Adv. Mater.* **21**, 3668 (2009).
6. Q-F. Zhang, K. Park, J-T. Xi, D. Myers, and G-Z. Cao: Recent progress in dye-sensitized solar cells using nanocrystallite aggregates. *Adv. Energy Mater.* **1**, 988 (2011).
7. A. Mishra, M-K-R. Fischer, and P. Bäuerle: Metal-free organic dyes for dye-sensitized solar cells: From structure: Property relationships to design rules. *Angew. Chem. Int. Ed.* **48**, 2474 (2009).
8. G-L. Shang, J-H. Wu, M-L. Huang, J-M. Lin, Z. Lan, Y-F. Huang, and L-Q. Fan: Facile synthesis of mesoporous tin oxide spheres and their applications in dye-sensitized solar cells. *J. Phys. Chem. C* **116**, 20140 (2012).
9. B. O'Regan, K. Bakker, J. Kroeze, H. Smit, P. Sommeling, and J-R. Durrant: Measuring charge transport from transient photovoltage rise times. A new tool to investigate electron transport in nanoparticle films. *J. Phys. Chem. B* **110**, 17155 (2006).
10. S. Sodergren, A. Hagfeldt, J. Olsson, and S-E. Lindquist: Theoretical models for the action spectrum and the current-voltage characteristics of microporous semiconductor films in photoelectrochemical cells. *J. Phys. Chem.* **98**, 5552 (1994).
11. K. Pan, Y. Dong, W. Zhou, G. Wang, Q. Pan, Y. Yuan, X. Miao, and G. Tian: TiO_2-B nanobelt/anatase TiO_2 nanoparticle heterophase nanostructure fabricated by layer-by-layer assembly for high-efficiency dye-sensitized solar cells. *Electrochim. Acta* **88**, 263 (2013).
12. A. Martinson, M. Goes, F. Fabregat-Santiago, J. Bisquert, M. Pellin, and J. Hupp: Electron transport in dye-sensitized solar cells based on ZnO nanotubes: Evidence for highly efficient charge collection and exceptionally rapid dynamics. *J. Phys. Chem. A* **113**, 4015 (2009).
13. L. Yang and W. Leung: Application of a bilayer TiO_2 nanofiber photoanode for optimization of dye-sensitized solar cells. *Adv. Mater.* **23**, 4559 (2011).
14. Z.Y. Liu and M. Misra: Dye-sensitized photovoltaic wires using highly ordered TiO_2 nanotube arrays. *ACS Nano* **4**, 2196 (2010).
15. G. Zhang, K. Pan, W. Zhou, Y. Qu, Q. Pan, B. Jiang, G. Tian, G. Wang, Y. Xie, Y. Dong, X. Miao, and C. Tian: Anatase TiO_2 pillar–nanoparticle composite fabricated by layer-by-layer assembly for high-efficiency dye-sensitized solar cells. *Dalton Trans.* **41**, 12683 (2012).
16. B. Tan and Y. Wu: Dye-sensitized solar cells based on anatase TiO_2 nanoparticle/nanowire composites. *J. Phys. Chem. B* **110**, 15932 (2006).
17. M. Yang, H. Jha, N. Liu, and P. Schmuki: Increased photocurrent response in Nb-doped TiO_2 nanotubes. *J. Mater. Chem.* **21**, 15205 (2011).
18. K. Zhu and A-J. Frank: Converting light to electrons in oriented nanotube arrays used in sensitized solar cells. *MRS Bull.* **36**, 446 (2011).

https://doi.org/10.1557/jmr.2014.50 Published online by Cambridge University Press

19. J. Wang and Z-Q. Lin: Dye-sensitized TiO_2 nanotube solar cells with markedly enhanced performance via rational surface engineering. *Chem. Mater.* **22**, 579 (2010).
20. M. Yang, D. Kim, H. Jha, K. Lee, J. Paul, and P. Schmuki: Nb doping of TiO_2 nanotubes for an enhanced efficiency of dye-sensitized solar cells. *Chem. Commun.* **47**, 2032 (2011).
21. P-T. Hsiao, Y-J. Liou, and H. Teng: Electron transport patterns in TiO_2 nanotube arrays based dye-sensitized solar cells under frontside and backside illuminations. *J. Phys. Chem. C* **115**, 15018 (2011).
22. M. Paulose, K. Shankar, O-K. Varghese, G-K. Mor, B. Hardin, and C-A. Grimes: Backside illuminated dye-sensitized solar cells based on titania nanotube array electrodes. *Nanotechnology* **17**, 1446 (2006).
23. M. Paulose, K. Shankar, O-K. Varghese, G-K. Mor, and C-A. Grimes: Application of highly-ordered TiO_2 nanotube-arrays in heterojunction dye-sensitized solar cells. *J. Phys. D: Appl. Phys.* **39**, 2498 (2006).
24. P. Roy, D. Kim, K. Lee, E. Spiecker, and P. Schmuki: TiO_2 nanotubes and their application in dye-sensitized solar cells. *Nanoscale* **2**, 45 (2010).
25. Z. Liu, X. Zhang, S. Nishimoto, M. Jin, D-A. Tryk, T. Murakami, and A. Fujishima: Highly ordered TiO_2 nanotube arrays with controllable length for photoelectrocatalytic degradation of phenol. *J. Phys. Chem. C* **112**, 253 (2008).
26. K. Shankar, G-K. Mor, A. Fitzgerald, and C-A. Grimes: Cation effect on the electrochemical formation of very high aspect ratio TiO_2 nanotubes in formamide-water mixtures. *J. Phys. Chem. C* **111**, 21 (2007).
27. L. Qi, Y. Ma, Q. Ouyang, Y. Zhang, L. Li, and Y. Chen: The controllable synthesis of chain-like TiO_2 networks with multiwalled carbon nanotubes as templates and its application for dye-sensitized solar cells. *J. Nanopart. Res.* **14**, 907 (2012).
28. G-K. Mor, K. Shankar, M. Paulose, O-K. Varghese, and C-A. Grimes: Enhanced photocleavage of water using titania nanotube arrays. *Nano Lett.* **5**, 191 (2005).
29. K. Pan, Y-Z. Dong, C-G. Tian, W. Zhou, G-H. Tian, B-F. Zhao, and H-G. Fu: TiO_2-B narrow nanobelt/TiO_2 nanoparticle composite photoelectrode for dye-sensitized solar cells. *Electrochim. Acta* **54**, 7350 (2009).
30. C. Longo, A-F. Nogueira, M-A. De Paoli, and H. Cachet: Solid-state and flexible dye-sensitized TiO_2 solar cells: a study by electrochemical impedance spectroscopy. *J. Phys. Chem. B* **106**, 5925 (2002).

Supplementary Material

To view supplementary material for this article, please visit http://dx.doi.org/jmr.2014.50.

https://doi.org/10.1557/jmr.2014.50 Published online by Cambridge University Press